



Swansea University  
Prifysgol Abertawe



## Cronfa - Swansea University Open Access Repository

---

This is an author produced version of a paper published in:

*JOM*

Cronfa URL for this paper:

<http://cronfa.swan.ac.uk/Record/cronfa34759>

---

### **Paper:**

Kish, J., Birbilis, N., McNally, E., Glover, C., Zhang, X., McDermid, J. & Williams, G. (2017). Corrosion Performance of Friction Stir Linear Lap Welded AM60B Joints. *JOM*

<http://dx.doi.org/10.1007/s11837-017-2504-6>

---

This item is brought to you by Swansea University. Any person downloading material is agreeing to abide by the terms of the repository licence. Copies of full text items may be used or reproduced in any format or medium, without prior permission for personal research or study, educational or non-commercial purposes only. The copyright for any work remains with the original author unless otherwise specified. The full-text must not be sold in any format or medium without the formal permission of the copyright holder.

Permission for multiple reproductions should be obtained from the original author.

Authors are personally responsible for adhering to copyright and publisher restrictions when uploading content to the repository.

<http://www.swansea.ac.uk/iss/researchsupport/cronfa-support/>

# Corrosion Performance of Friction Stir Linear Lap Welded AM60B Joints

J.R. Kish<sup>1</sup>, N. Birbilis<sup>2</sup>, E.M. McNally<sup>1</sup>, C.F. Glover<sup>3</sup>, X. Zhang<sup>1</sup>,  
J.R. McDermid<sup>1</sup> and G. Williams<sup>3</sup>

<sup>1</sup>Centre for Automotive Materials and Corrosion, McMaster University, Hamilton, ON, Canada  
<sup>2</sup>Department of Materials Science and Engineering, Monash University, Clayton, VIC, Australia  
<sup>3</sup>Materials Research Centre, College of Engineering, Swansea University, Swansea, UK

\*Corresponding Author: [kishjr@mamcaster.ca](mailto:kishjr@mamcaster.ca) | 905-525-9140

A corrosion investigation of friction stir linear lap welded AM60B joints used to fabricate an Mg alloy-intensive automotive front end sub-assembly was performed. The stir zone exhibited a slightly refined grain size and significant break-up and re-distribution of the divorced Mg<sub>17</sub>Al<sub>12</sub> ( $\beta$ -phase) relative to the base material. Exposures in NaCl (aq) environments revealed that the stir zone was more susceptible to localized corrosion than the base material. Scanning vibrating electrode technique (SVET) measurements revealed differential galvanic activity across the joint. Anodic activity was confined to the stir zone surface and involved initiation and lateral propagation of localized filaments. Cathodic activity was initially confined to the base material surface, but was rapidly modified to include the cathodically-activated corrosion products in the filament wake. Site-specific surface analyses revealed that the corrosion observed across the welded joint was likely linked to variations in Al distribution across the surface film/metal interface.

## INTRODUCTION

Lightweighting as a means to improve fuel economy to meet regulatory requirements is of considerable interest to the automotive industry.<sup>1</sup> For example, a 7% improvement in fuel economy can be achieved for each 10% reduction in vehicle weight depending on the size of the powertrain.<sup>2</sup> Despite the significant weight savings potential, Mg alloys remain under-utilized in multi-material structural applications due to challenges associated with processing (formability), assembly (joining) and in-service performance (corrosion).<sup>3,4</sup> A multi-national Mg front end research and development (MFERD) project was established to address aspects of these key challenges.<sup>5,6</sup> Mg alloy AM60B, produced by high pressure die casting (HPDC), and friction stir welding (FSW) were selected as a promising structural Mg alloy and joining technology, respectively, to fabricate both Mg-intensive and multi-material sub-assemblies for component-level testing.<sup>5-7</sup> A well-developed understanding of variations in the localized corrosion susceptibility across the friction stir welded is a critical step towards the utilization of FSW AM60B HPDC components in multi-material assemblies.

Well-developed corrosion of multi-phase Mg-Al (AM<sub>xx</sub> and AZ<sub>xx</sub>) alloys in aqueous chloride-containing solutions is strongly affected by the heterogeneous nature of the alloy microstructure; including the size, shape and distribution of secondary intermetallic phases.<sup>8-15</sup> Arguably, the Al distribution within the microstructure is the most important factor in controlling corrosion as regions deficient in Al corrode at significantly higher rates.<sup>16-18</sup> The multi-phase microstructure is particularly susceptible to micro-galvanic corrosion with the more noble Al-rich phases serving as local cathodes.<sup>19-21</sup> Al-rich phases also can locally alter the surface film

and, thus, regulate the local cathodic activity as Al enrichment occurs.<sup>16-18,22</sup> However, the ability of the sub-surface Al distribution and any associated Al enrichment layer to alter the surface film to avoid cathodic activation has not been investigated in a unified context. The scanning vibrating electrode (SVET) technique has eloquently revealed that breakdown of Mg<sup>23,24</sup> and single phase Mg-Al alloys<sup>25-27</sup> in NaCl (aq) electrolytes involves laterally-spreading focal anodes that leave behind cathodically-activated corrosion products. Thus, identifying microstructural features that can alter surface films to avoid cathodic activation is desirable from a corrosion performance perspective.

Friction stir welding of AM60B castings has been shown to significantly alter the microstructure of the base material. The stir zone typically contains a recrystallized equiaxed stir zone within which the divorced eutectic  $\beta$ -phase is broken-up and re-distributed, whereas the Al<sub>x</sub>Mn<sub>y</sub> phase remains virtually unchanged.<sup>28-31</sup> Thus, the goal of the current work was to link critical aspects of microstructural variation on the intrinsic corrosion performance across a friction stir linear lap welded HPDC AM60B joints of interest to the automotive industry.

## EXPERIMENTAL PROCEDURES

Friction stir linear lap welded AM60B joints were prepared from front end sub-assemblies provided in the as-welded condition by General Motors Global Research and Development Center (Warren, Michigan, Fig. 1a). Specific details pertaining to the friction stir welding set-up and procedure used are published elsewhere.<sup>32</sup> All samples were taken from welds joining the HPDC AM60B shock tower casting (3.2 mm at joint location) to the Mg alloy AM30 (3 mm) lower rail extrusion. Isolated cross-sectional base material and stir zone samples were cold-mounted in epoxy, prepared using standard metallographic procedures and examined using both light optical microscopy and scanning electron microscopy (JEOL 6610LV) equipped with X-ray energy dispersive spectroscopy (EDS) (Oxford Instruments with AZtecEnergy software). The imaging and EDS line profiles were acquired using a 12 keV acceleration voltage and a 10 mm working distance.

SVET measurements of the friction stir linear lap welded joint surface were carried out using instrumentation of in-house construction, described in detail elsewhere.<sup>23</sup> The vibrating probe consisted of a 125  $\mu\text{m}$  diameter platinum wire encased in a glass sheath such that the electrode at the probe tip comprised a Pt micro-disc. The vertically orientated probe was held at a height of 100  $\mu\text{m}$  over the corroding surface of interest and vibrated at an amplitude of  $\pm 10 \mu\text{m}$  at a frequency of 140 Hz. The-derived SVET peak-to-peak voltage ( $V_{pp}$ ) signal was converted to values of current flux density along the axis of probe vibration ( $j_z$ ) after galvanostatic calibration using a two compartment cell containing 5% w/v NaCl (aq).<sup>23,33</sup> By rastering the probe over the corroding surface and logging values of  $V_{pp}$  at user-defined co-ordinates, a spatially resolved map of  $j_z$  values was compiled.

The joint sample used for this purpose was abraded to produce a completely flat, polished surface, starting with coarse grit SiC paper and working through to a fine 2400 grit finish. Finally, the surface was washed with an aqueous surfactant and rinsed with distilled water followed by ethanol. A working electrode area consisting of the base material and stir zone was isolated by masking the sample with 90  $\mu\text{m}$  thick extruded PTFE tape (3M 5490), such that a 27 mm  $\times$  4 mm region comprising equal areas of the base material and stir zone was exposed. The sample was subsequently immersed, exposed area uppermost, in room temperature 5 wt.% NaCl (aq) electrolyte. The working surface was scanned immediately following immersion, and at

approximately 1-h intervals thereafter during the 18 h exposure. Open-circuit potential (OCP) measurements were also recorded on isolated surface areas (10 mm × 10 mm) of the base material and stir zone upon exposure to the 5 wt.% NaCl (aq) electrolyte.

Isolated base material and stir zone samples (10 mm × 10 mm) were mechanically abraded using 2400 grit SiC paper and rinsed with ethanol in preparation for exposure to room temperature 3.5 wt.% NaCl (aq) electrolyte for 24 h. After exposure, the base material and stir zone samples were rinsed with distilled water to remove excess electrolyte and then ethanol (to promote fast drying). A Zeiss NVision 40 dual beam focused ion beam (FIB)-SEM was used to prepare thin foil cross-sections of the intact surface film for subsequent examination using transmission electron microscopy (TEM). A protective W layer was deposited at the site of interest prior to FIB milling. The resultant foils were examined at cryogenic temperatures in a FEI Titan 80-300 LB TEM operating at an acceleration voltage of 200 keV. EDS maps were acquired in scanning TEM (STEM) mode using an Oxford Inca Si(Li) EDS detector. Images were collected using the Gatan Digital Micrograph software and EDS data was analyzed using Oxford's INCA software

## RESULTS

A macroscopic cross-sectional image of the overlapping welded joint (Fig. 1b) shows a sound stir zone with sufficient penetration through the AM60B casting into the AM30 extrusion. The cross-sectional images of the base material (Fig. 1c) and stir zone (Fig. 1d) shows that friction stir welding significantly modified the starting AM60B microstructure. The base material exhibited the fully divorced eutectic morphology with the grain boundaries consisting of  $\beta$ -phase ( $\text{Mg}_{17}\text{Al}_{12}$ ) particles surrounded by a network of Al-enriched eutectic  $\alpha$ -phase.<sup>34</sup> Not shown in the image are the casting porosity and the randomly distributed  $\text{Al}_x\text{Mn}_y$  intermetallic particles. The stir zone (Fig. 1d) appears to be a single phase structure comprised of recrystallized grains, which have been refined relative to the base material. The casting porosity originally present in the base material was effectively eliminated. The bulk composition (major alloying elements) of the base material and stir zone listed in Fig. 1c and 1d, as determined using inductively coupled plasma - mass spectroscopy (ICP-MS), showed essentially no dilution of the Al and Mn concentration in the stir zone. Although not reported here, the (mechanically-abraded) surface of the base material and stir zone was analyzed using both X-ray photoelectron spectroscopy (XPS) and Auger electron spectroscopy (AES). Heavy metal (Fe) contamination was not found on either surface, thus discounting this as being a possible factor affecting the relative corrosion across the joint.

Fig. 2 shows backscatter electron (BSE) images documenting typical the fine-scale microstructure of the base material and stir zone. Also included are associated EDS compositional profiles corresponding to the lines superimposed onto the BSE images. The Al content in the base material varied significantly along the profile, which reflects Al depletion (relative to the bulk) in the center of the grains and Al enrichment (relative to the bulk) on the grain boundaries. The grain boundary Al enrichment corresponds to the fully divorced eutectic structure:  $\beta$ -phase ( $\text{Mg}_{17}\text{Al}_{12}$ ) particles connected by a network of Al-enriched eutectic  $\alpha$ -phase (light grey network in Fig. 2a). Several of the Al enrichment spikes coincided with significant Mn enrichment (relative to the bulk), indicating the presence of an  $\text{Al}_x\text{Mn}_y$  particle at that location (bright particles in Fig. 2a). The Al content in the stir zone showed a more uniform distribution along the profile. The single Al enrichment spike in the profile coincided with

significant Mn enrichment (relative to the bulk), indicating the presence of an  $\text{Al}_x\text{Mn}_y$  particle at that location (bright particles in Fig. 2b). Fig. 3 shows a set of elemental maps acquired from the stir zone at higher magnification. The Al content (Fig. 3c) showed some variation in the stir zone as local regions of depletion (relative to the bulk) are evident. The bright particles in Fig 3a coincided with both Al (Fig 3c) and Mn (Fig. 3d) enrichment, indicating  $\text{Al}_x\text{Mn}_y$  particles at those locations.

Fig. 4 shows a series of SVET-derived  $j_z$  distribution maps recorded from the surface of the welded joint sample over an 18 h immersion period in the 5 wt.% NaCl (aq) electrolyte, along with a photographic image of the post-corrosion surface. Localized corrosion was initiated as filaments that propagated laterally across the surface. Repeated immersion experiments showed that the localized (dark) filament corrosion always initiated on the stir zone material with the adjoining base material surface being largely unaffected. The  $j_z$  distributions associated with propagating corrosion filaments showed that a strongly anodic leading edge ( $j_z = \text{ca } +50 \text{ A m}^{-2}$ ) left behind a cathodically-activated region ( $j_z = \text{ca. } -2 \text{ A m}^{-2}$ ) as it traversed the exposed surface of the stir zone. The estimated rate of filament propagation was  $0.2 \text{ mm h}^{-1}$  over the stir zone surface. The  $j_z$  distributions associated with the exposed base material surface showed consistent cathodic activity.

The predisposition of the stir zone to undergo breakdown in preference to the base material was checked by measuring the OCP transient following initial immersion. The point of breakdown of Mg and selected alloys in NaCl (aq) electrolytes can be identified by a local maximum in the OCP transient following immersion, marking the breakdown potential ( $E_b$ ).<sup>35</sup> It was further demonstrated that the  $E_b$  is highly dependent upon chloride ion concentration and that the value of  $E_b$  can be used as a measure of the resistance of Mg to localized corrosion initiation and subsequent cathodic activation [ref]. The OCP transients of the isolated base material and stir zone following immersion in 5 wt. % NaCl (aq) electrolyte are shown in Fig. 5 along with photographic images of the samples after 24 h immersion in a 3.5 wt.% NaCl (aq) electrolyte. While each transient clearly exhibited a characteristic local maximum at the point of breakdown, the value of  $E_b$  was 20 mV more negative for the stir zone in comparison with the base material, signifying a greater tendency to undergo breakdown under the same conditions. The time to achieve  $E_b$  was shorter for the stir zone, also signifying a greater tendency to undergo breakdown under the same conditions. Post exposure images (Fig. 5c and 5d) show that corrosion on both surfaces involved the initiation and propagation of localized dark filaments.

Fig. 6a and 6b show a bright field image of the intact film formed on the base material and stir zone surface, respectively, in cross-section after 24 h immersion in 3.5 wt.% NaCl (aq). The intact film formed on both materials is relatively thin ( $\sim 400 \text{ nm}$ ) and reasonably compact, relative to the much thicker and more defective corrosion product that is the dark corrosion product filament on Mg-Al alloys.<sup>26,36</sup> Although not shown here, selected area diffraction (SAD) patterns collected from the both intact surface films are consistent in part with crystalline MgO. Typical EDS maps associated with the intact film of the base material and stir zone is shown in Fig. 6c and 6d, respectively. Both films are comprised largely of Mg and O, consistent with the SAD results. Regions of significant Al enrichment are observed sub-surface in both materials. The single Al-enriched region in the base material is not concomitantly enriched with Mn, which signifies the presence of a  $\beta$ -phase particle near the metal/film interface. Similarly, two of the three Al-enriched regions in the stir zone are not concomitantly enriched with Mn, signifying the presence of  $\beta$ -phase particles. Noting the difference in scale, the  $\beta$ -phase particles in the stir zone were significantly smaller versus the base material, but present nonetheless.

A typical EDS line profile of the Al content across the film/metal interface of each material (Fig. 7a and 7b) is presented in Fig. 7c. Care was taken to ensure the line profiles did not include  $\beta$ -phase particles. Far removed from the interface within the bulk material, the Al intensity is similar for both materials. However, as the metal/film interface is approached, there is a significant Al enrichment zone in the base material that does not exist in the stir zone. There may be a narrow Al enrichment zone in the stir zone as indicated by the small intensity peak, but it is relatively insignificant in comparison to the bulk material. Al was also incorporated into the intact film formed on the base material, but was not as significantly incorporated into the stir zone intact film.

## DISCUSSION

Immersion of friction stir welded AM60B joint samples in NaCl (aq) electrolytes revealed two key aspects that will affect their corrosion performance in multi-material assemblies: galvanic corrosion across the welded joint and the corrosion propagation morphology. Formation of the dark cathodically-activated filaments that initiate and propagate laterally across exposed surfaces is consistent with the behavior exhibited by other Mg-Al alloys immersed in similar electrolytes.<sup>Error! Bookmark not defined.-27</sup> The more surprising aspect is that localized filament corrosion was restricted to the stir zone surface, at least for the immersion conditions studied. Both the OCP and  $E_b$  of the isolated stir zone are more negative (active) than the isolated base material (Fig. 4). Thus, the stir zone would serve as a cathode when in galvanic contact with the base material (as is the case for the friction stir welded joint studied herein). The resultant galvanic cell-induced anodic polarization of the stir zone would be sufficient to fix the mixed potential just above the associated  $E_b$  (stir zone), whereas the associated cathodic polarization of the base material would be sufficient to fix the mixed potential just below  $E_b$  (base material) for the immersion conditions studied. Cathodic activity is believed to have been initially confined to the base material surface, but quickly included the dark cathodically-activated corrosion products in the filament wake. The predisposition of the base material to continue to serve as a cathode after localized filament corrosion initiated on the stir zone was verified by SVET measurements on isolated base material (not reported here). Localized corrosion filaments were observed to initiate after ca. 10 minutes of immersion. The fact that localized corrosion did not initiate on the base material of the welded joint samples indicates that it was effectively cathodically-protected during immersion.

The tendency for the stir zone to serve as the anode is believed to be controlled by the increased tendency (more active  $E_b$ ) of the intact film to break down (i.e. cathodically activate). A significant difference in the Al distribution across the film/metal interface of the two materials was revealed by the TEM-EDS analysis. Consequently, it is believed that the Al distribution across the interface altered the ability of the intact film to avoid breakdown. The incorporation of chloride ions into the intact film on Mg<sup>Error! Bookmark not defined..39</sup> and Mg-Al alloys<sup>40</sup> is believed to be an important precursor step to breakdown: formation of more soluble hydroxy-chloride complexes.<sup>Error! Bookmark not defined..41</sup> The low Al content in the stir zone film suggests the film is consistent with a simple MgO/(Mg(OH)<sub>2</sub>) mixture<sup>39</sup> rather than a Mg-Al-type layered double hydroxide (LDH) compound such as meixerite [Mg<sub>6</sub>Al<sub>2</sub>(OH)<sub>18</sub>·4H<sub>2</sub>O] or hydrotalcite [Mg<sub>6</sub>Al<sub>2</sub>CO<sub>3</sub>(OH)<sub>16</sub>·4H<sub>2</sub>O].<sup>42</sup> It follows from the more active stir zone film  $E_b$  that the presumed MgO/(Mg(OH)<sub>2</sub>) intact film has a stronger tendency to form more soluble hydroxy-chloride complexes. Studies of the solubility of MgO/Mg(OH)<sub>2</sub> relative to Mg-Al-type LDH supports this

theory.<sup>43</sup> Al enrichment across the film/metal interface requires incongruent dissolution to occur prior to breakdown. Surface analysis of films formed on Mg-Al alloys during immersed in pure water have shown this to be the case.<sup>42,44-46</sup> It is believed that the Al distribution across the intact film/metal interface is controlled by the sub-surface microstructure. However, this link has not yet been investigated in a unified context. The  $\beta$ -phase morphology in the two microstructures differs significantly: micro-scale grain boundary particles in the base material versus nano-scale matrix particles in the stir zone. A similar change in  $\beta$ -phase morphology from micro-scale plates to nano-scale particles (produced by heat treatment) has been shown to affect the localized corrosion susceptibility of Mg alloy AZ91 in dilute NaCl (aq).<sup>12</sup> However, thus far, such assertions have tended to focus on the propensity for micro-galvanic corrosion based on local microstructure, without consideration of broader welded assemblies. The work herein, particularly in the context of welded assemblies, identified that local potentials are important in the determination of anodic and cathodic sites overall, whilst the ‘propagation’ of corrosion was dictated by the ability of corrosion to spread – which requires consideration of the critical breakdown of surface film and the extent of cathodic activation of the propagating localized corrosion products.

The results have two key implications associated with the use of friction stir welded liner lap joints to join HPDC AM60B components in multi-material assemblies. The first is the galvanic interaction that occurs across the welded joint, with the base material serving as the cathode and the stir zone serving as the anode. The stir zone will preferentially corrode, which will likely result in enhanced degradation of thin-walled HDPC components. The second is the corrosion propagation morphology, which involves laterally spreading filaments. As a protective coating scheme would be applied in practice, these laterally-spreading corrosion filaments will likely cause coating delamination. More research focused on understanding the risk of coating delamination from filament corrosion and subsequent galvanic activity of friction stir linear lap welded AM60B joints is warranted.

## CONCLUSIONS

1. Friction stir linear lap welding of Mg alloy AM60B significantly altered the base material microstructure. The major alteration reported in this study was the change in the  $\beta$ -phase morphology: micro-scale grain boundary network in the base material versus distributed nano-scale particles in the stir zone. This change in local microstructure led to a change in the unique local potential, lowering the potential of the stir zone and rendering it a local anode in the context of the overall weld assembly.
2. Scanning vibrating probe measurements revealed that the stir zone was more susceptible to corrosion, which occurred in this case as laterally spreading localized filaments. The relative values of the open-circuit and breakdown potentials validate a galvanic interaction between the base material (cathode) and stir zone (anode) that accelerated localized corrosion of the stir zone.
3. This work reveals that conventional wisdom in first order consideration of dissimilar metal or weld metal induced corrosion are not the only (or key) factor in the case of corrosion of Mg-alloy assemblies. The corrosion propagation morphology and attendant rate are of particular importance, as indicated herein.

4. The tendency for the stir zone to serve as the anode is believed to be controlled by the increased tendency (more active  $E_p$ ) for the intact film to break down (cathodically activate). The Al distribution across the film/metal interface, influenced by the sub-surface microstructure, is believed to alter the ability of an intact film to avoid breakdown. Key microstructure features include both  $\beta$ -phase morphology and solute distribution within the matrix phase.

## **ACKNOWLEDGEMENTS**

We thank the Automotive Partnerships Canada (APC) program for providing financial support and the Magnesium Front End Research and Development (MFERD) partnership for providing the front end sub-assemblies for testing.

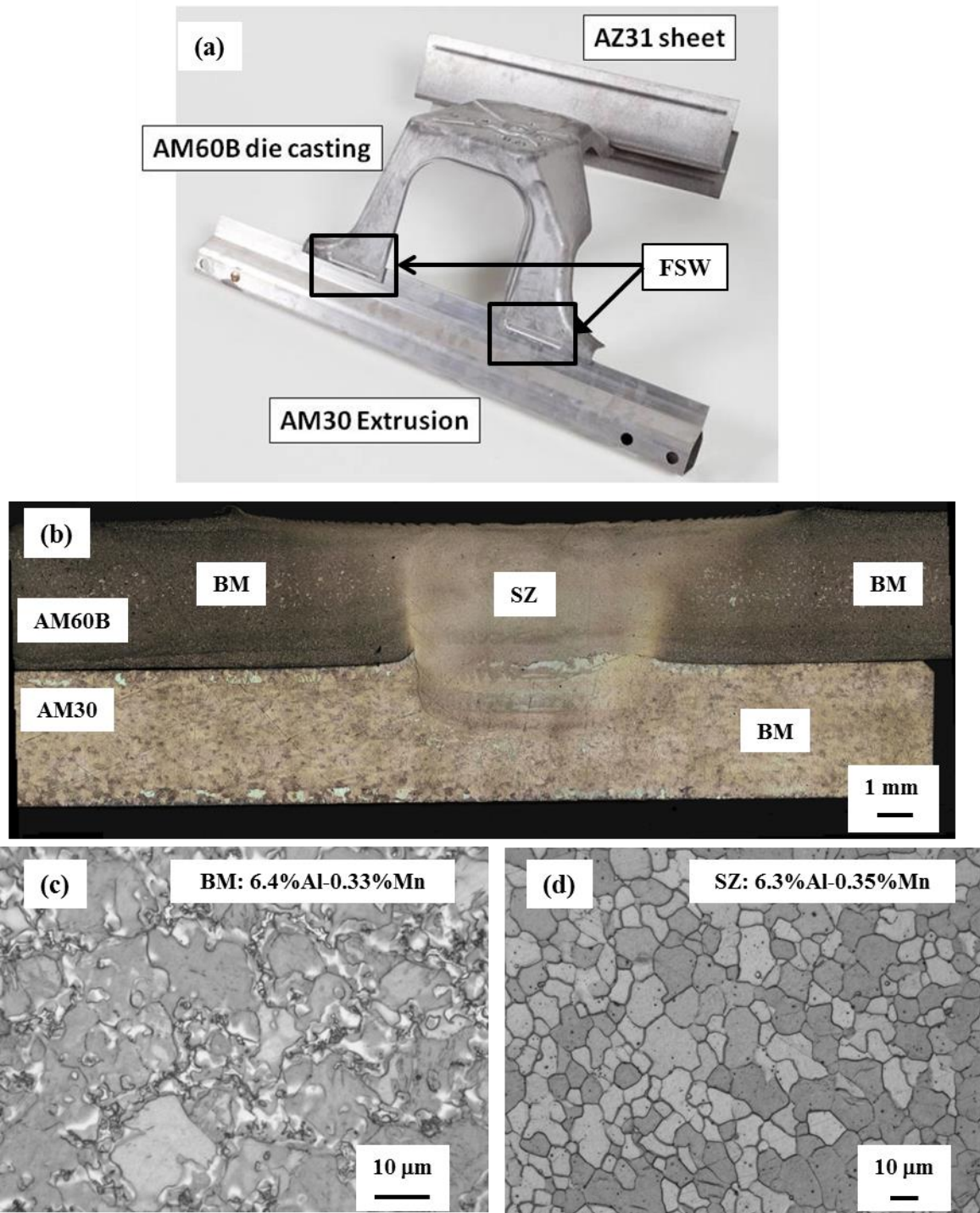


**Fig. 1.** (a) Photograph (courtesy of United States Automotive Materials Partnership LLC) of a front end shock tower sub-assembly. Arrows identify the friction stir linear lap welded AM60B joints of interest to this study. The length of the AZ31B sheet upper rail and the extruded AM30 lower rail are 46 cm and 84 cm, respectively. Light optical microscopy images of (b) welded joint in cross-section, (c) base material (BM) in cross-section and (d) stir zone (SZ) in cross-section.

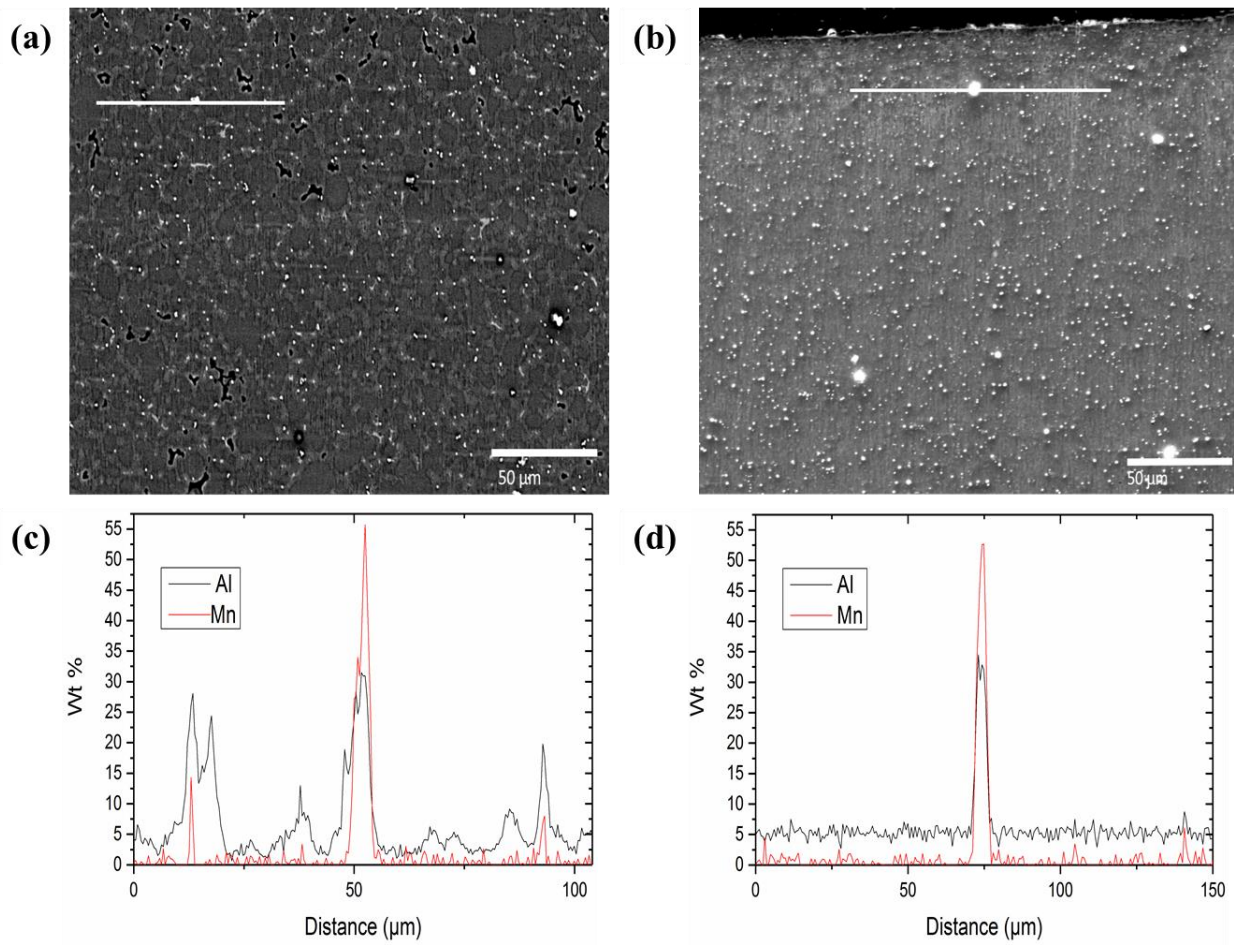


**Fig. 2.** SEM cross-sectional images of the microstructure and associated EDS line scans corresponding to the line superimposed on the image: (a) backscattered image of the base material and (b) secondary electron image of the stir zone. EDS Al and Mn compositional profiles in (c) base material and (d) stir zone.

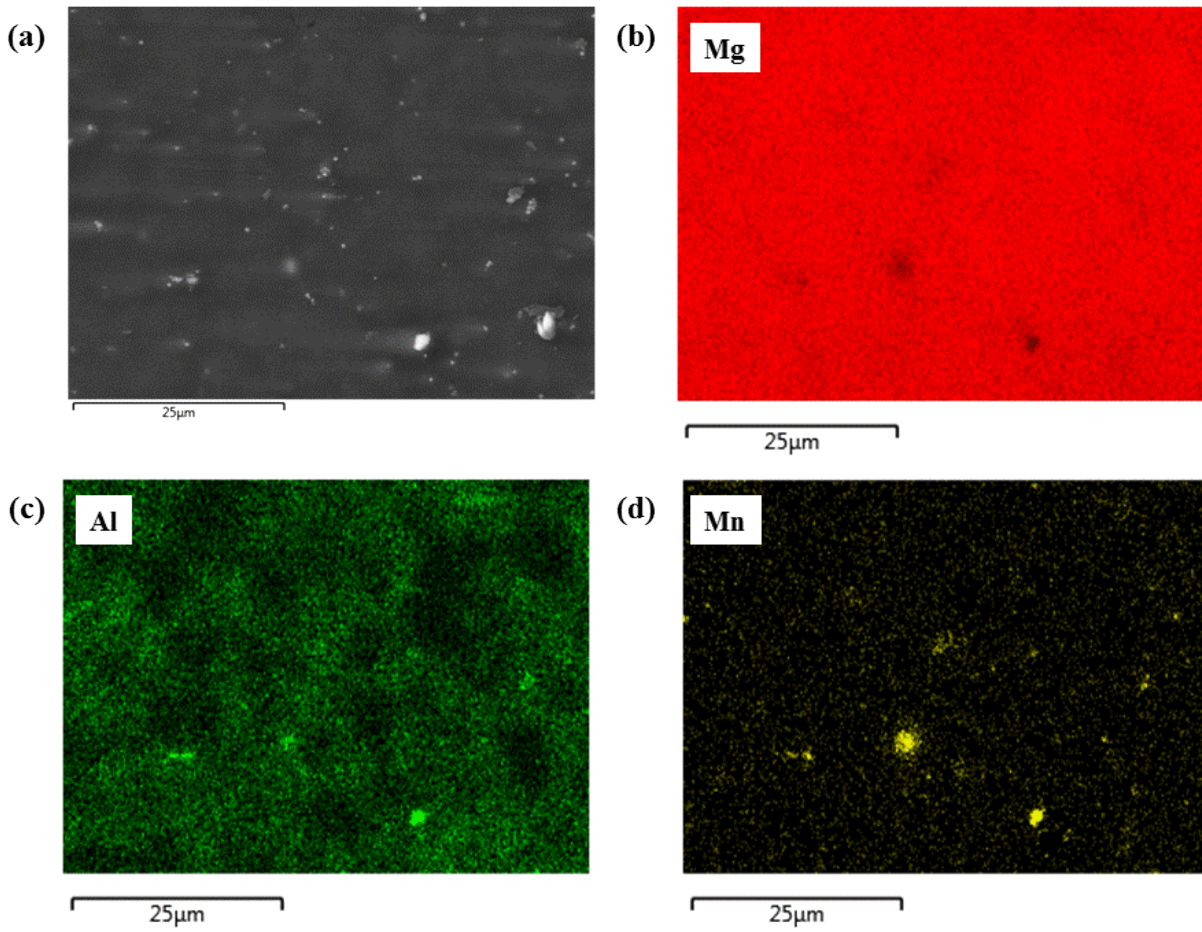


**Fig. 3.** SEM-EDS analysis of stir zone at higher magnification: (a) secondary electron image of mapped region, (b) Mg map, (c) Al map and (d) Mn map.

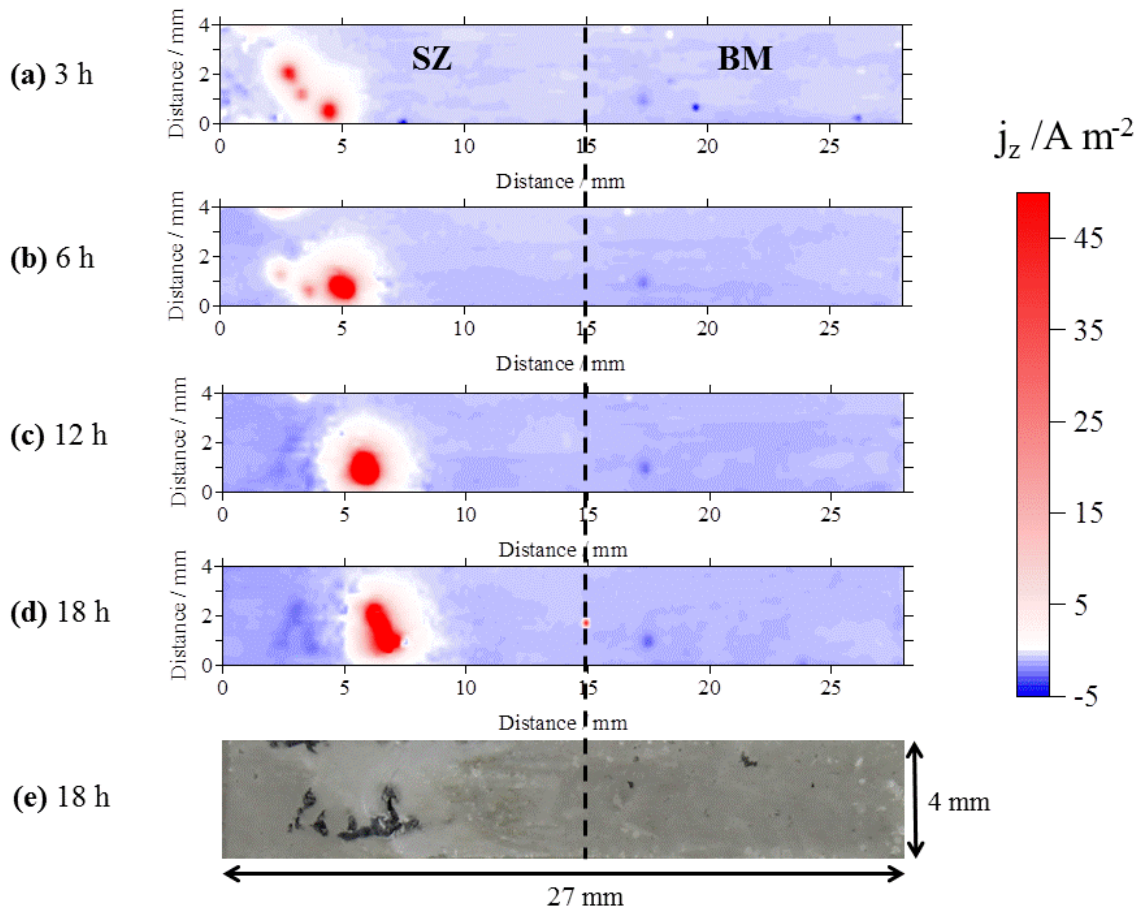


**Fig. 4.** (a-d) Series of SVET-derived  $j_z$  distribution maps recorded from the surface of the welded joint sample over an 18 h immersion in a 5 wt.% NaCl (aq) electrolyte, (e) along with a photographic image of the post-corrosion surface.

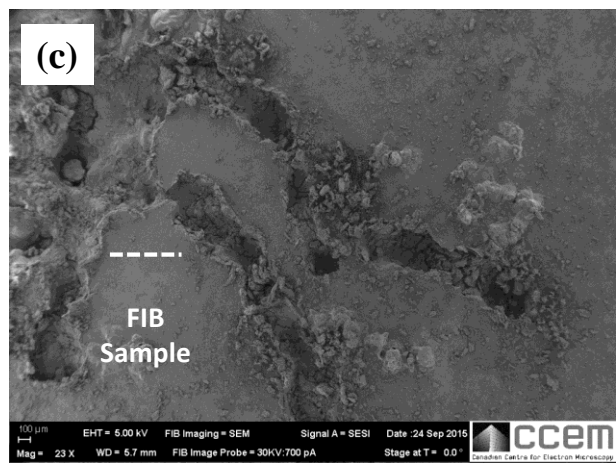
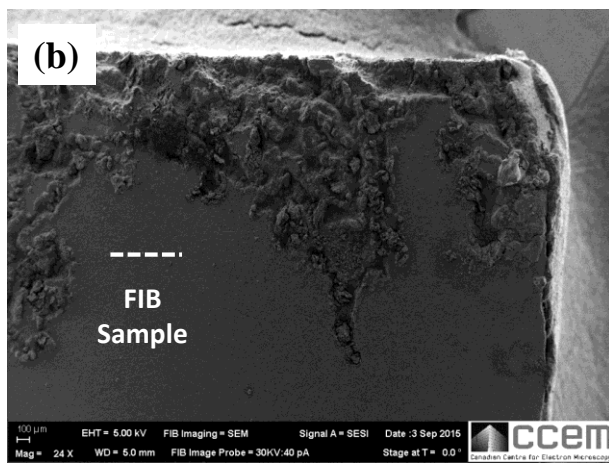
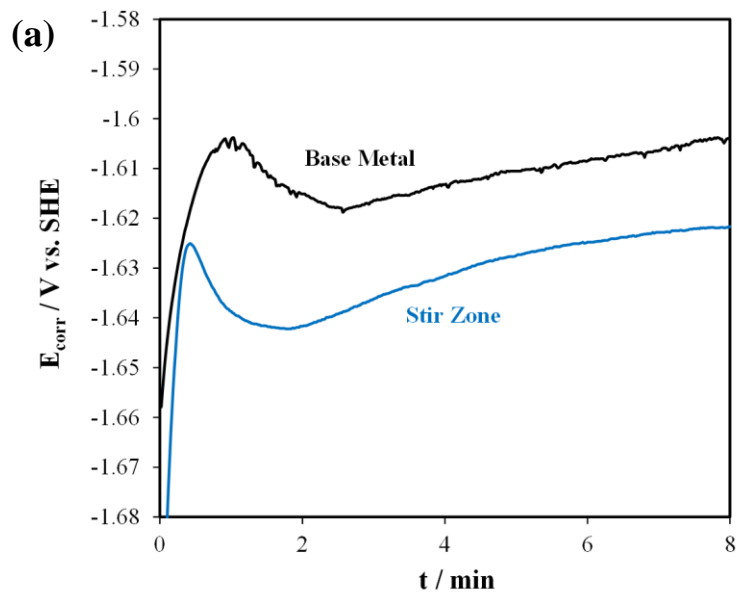


**Fig. 5.** (a) Open-circuit potential transients of isolated base material and stir zone samples recorded during exposure in 5 wt.% NaCl (aq). SEM image showing the filament corrosion formed on isolated (b) base material and (c) stir zone samples after 24 h exposure in 3.5 wt.% NaCl (aq) and associated sites of TEM sample extraction via FIB milling.

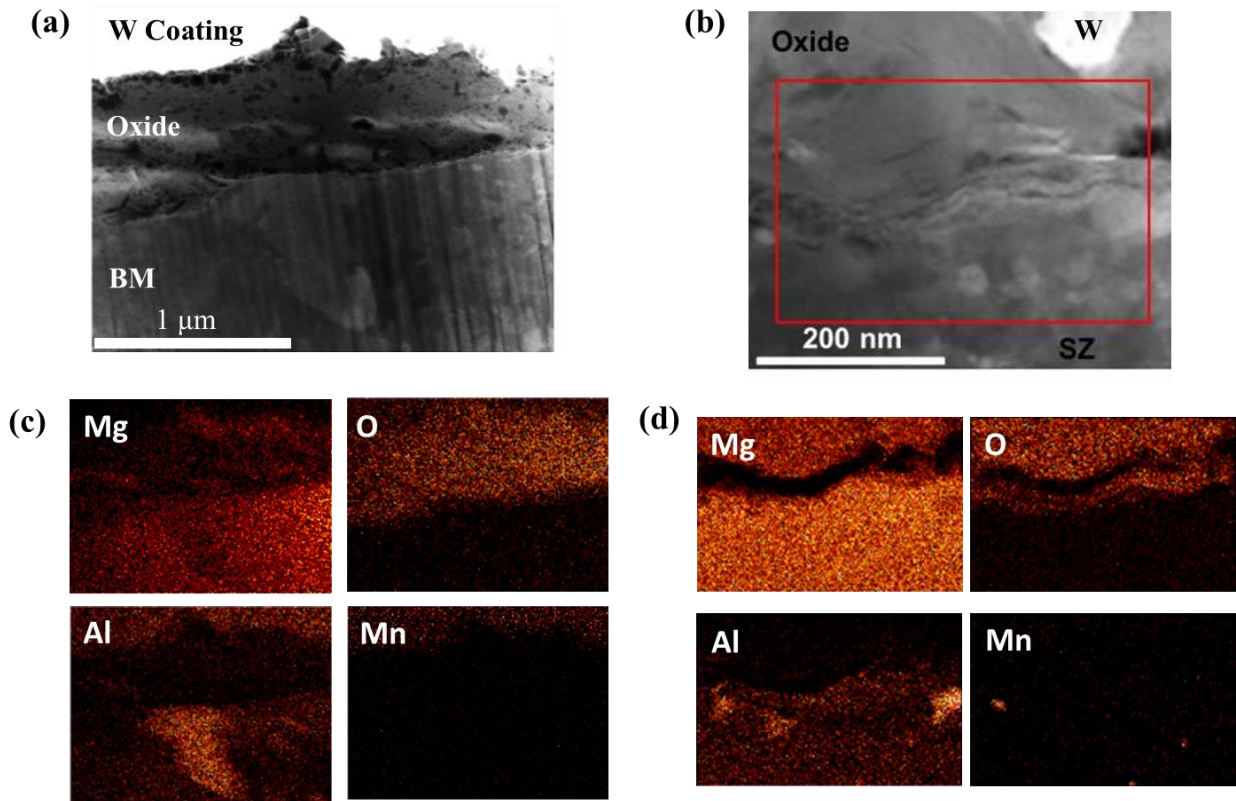


**Fig. 6.** Bright-field TEM cross-sectional image of intact film formed on the (a) base material and (b) stir zone after 24 h exposure in 3.5 wt.% NaCl (aq). Associated set of EDS maps of the film/metal interface of the (c) base material and (d) stir zone. The set of EDS maps in (d) correspond to the framed area in (b).

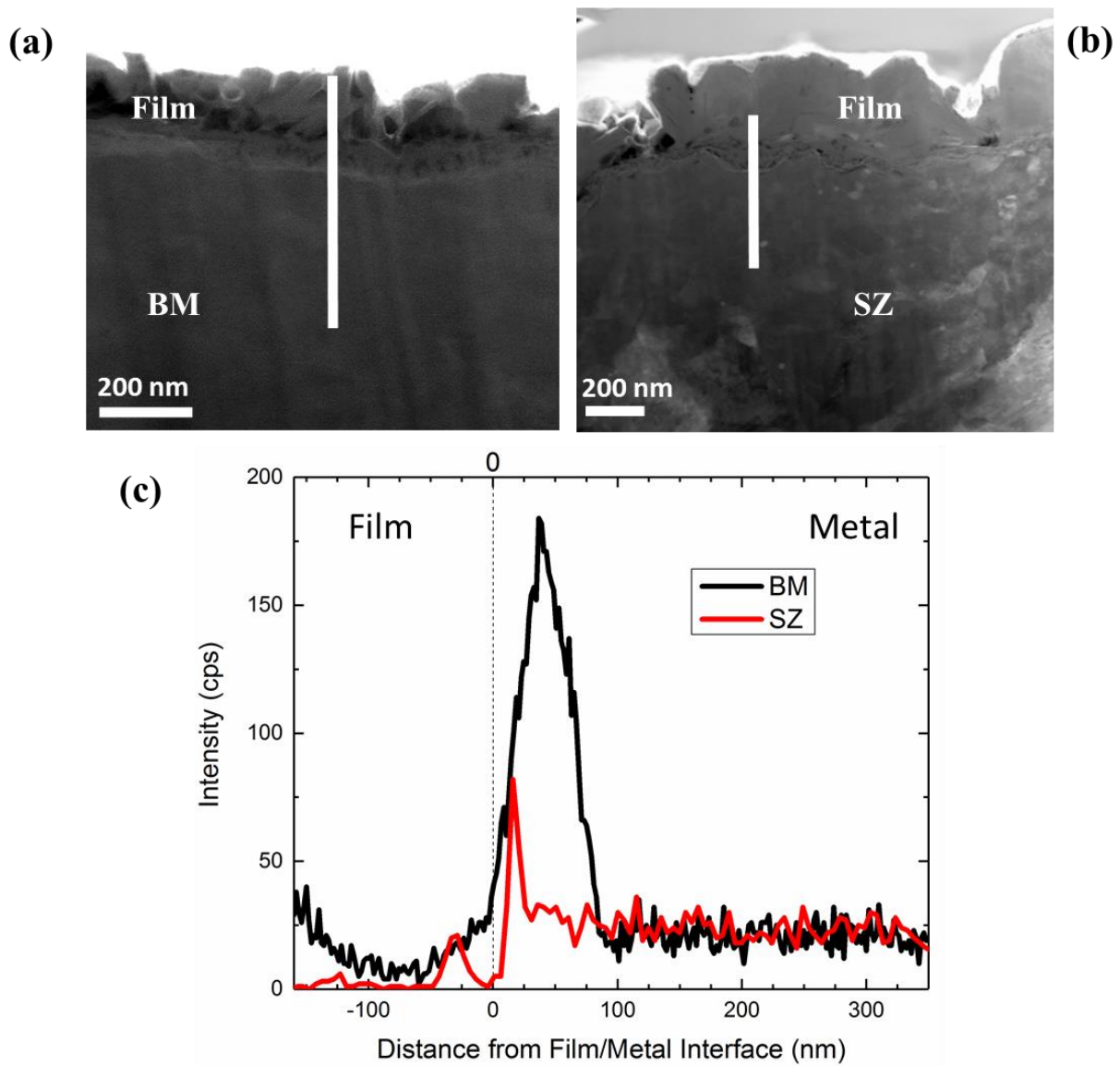


**Fig. 7.** Bright-field TEM cross-sectional image of intact film formed on the (a) base material and (b) stir zone after 24 h exposure in 3.5 wt.% NaCl (aq). (c) Plot of the associated EDS Al concentration profiles across film/metal interface.

## REFERENCES

- 1 T.B. Abbott, *Corrosion*, 71(2), 120 (2014).
- 2 W.J. Joost, *JOM*, 64(9), 1032 (2012).
- 3 W.J. Joost and P.E. Krajewski, *Scripta Materialia*, 128, 107 (2017).
- 4 M.P. Brady, W.J. Joost and C.D. Warren, *Corrosion*, 73(5), 452 (2017).
- 5 A.A. Luo, E.A. Nyberg, K. Sadayappan and W. Shi, *Adv. Mater. Perform.*, 166(10) 35 (2008).
- 6 A.A. Luo, E.A. Nyberg, K. Sadayappan, and W. Shi, in *Magnesium Technology*, ed. M.O. Pegguleryuz, N.R. Neelameggham, R.S. Beals, and E.A. Nyberg, (Warrendale, PA: TMS, 2008), p. 3.
- 7 R.C. McCune, J. Forsmark, B. Schneider, A. Luo, H. Gu, W. Schumacher, X. Chen, F. Vartolas, *SAE Int. J. Mater. Manf.*, 6(2), 242 (2013).
- 8 N. Pebere, C. Riera, and F. Dabosi, *Electrochim. Acta*, 35, 555 (1990).
- 9 T. Beldjoudi, C. Fiaud, and L. Robbiola, *Corrosion*, 49(9), 738 (1993).
- 10 G. Song, A. Atrens, X. Wu, and B. Zhang, *Corros. Sci.*, 40(10), 1769 (1998).
- 11 R.K. Singh Raman, *Metall. Mat. Trans. A*, 35(8), 2521 (2004).
- 12 M. Zhao, M. Liu, G. Song, and A. Atrens, *Corros. Sci.*, 50, 1939 (2008).
- 13 A. Pardo, M.C. Merino, A.E. Coy, F. Viejo, R. Arrabal, and S. Feliú, *Electrochim. Acta*, 53(27), 7890 (2008).
- 14 L.G. Bland and J.R. Scully, *Corrosion*, 73(5), 526 (2017).
- 15 R.K. Singh Raman, N. Birbilis, and J. Efthimiadis, *Corros. Eng. Sci. Technol.*, 39, 4 (2004).
- 16 R.M. Asmussen, P. Jakupi, M. Danaie, G.A. Botton, and D.W. Shoesmith, *Corros. Sci.*, 75, 114 (2013).
- 17 M. Danaie, R.M. Asmussen, P. Jakupi, D.W. Shoesmith, and G.A. Botton, *Corros. Sci.*, 77, 151 (2013).
- 18 R.M. Asmussen, W.J. Binns, P. Jakupi, and D. Shoesmith, *J. Electrochem. Soc.*, 161(10), C501 (2014).

- 19 O. Lunder, J.E. Lein, T.K. Aune, and K. Nisancioglu, *Corros. Sci.*, 45, 9 (1989).
- 20 A.D. Südholz, N.T. Kirkland, R.G. Buchheit, and N. Birbilis, *Electrochem. Solid-State Letters*, 14(2), C5 (2011).
- 21 L.G. Bland, N. Birbilis, and J.R. Scully, *J. Electrochem. Soc.*, 163(14) C895 (2016).
- 22 M. Danaie, R.M. Asmussen, P. Jakupi, D.W. Shoesmith, and G.A. Botton, *Corros. Sci.*, 83, 299 (2014).
- 23 G. Williams and H.N. McMurray, *J. Electrochem. Soc.*, 155(7), C340 (2008).
- 24 S. Fajardo, C.F. Glover, G. Williams, and G.S. Frankel, *Corrosion*, 73(5), 482 (2017).
- 25 G. Williams, H. Dafydd, and R. Grace, *Electrochim. Acta*, 109, 489 (2013).
- 26 Z.P. Cano, J.R. McDermid, and J.R. Kish, *J. Electrochem. Soc.*, 162, C732 (2015).
- 27 Z.P. Cano, J.R. Kish, and J.R. McDermid, *J. Electrochem. Soc.*, 163(3), C62 (2016).
- 28 J.A. Esparza, W.C. Davis, and L.E. Murr, *J. Mater. Sci.*, 38, 941 (2003).
- 29 M. Santella, A. Frederick, C. Degen, and T-Y. Pan, *JOM*, 58(5), 56 (2006).
- 30 P. Cavaliere, P.P. De Marco, *J. Mater. Sci.*, 41, 3459 (2006).
- 31 J. Robson, S. Cui, and Z. Chen, *Mater. Sci. Forum*, 654-656, 751 (2010).
- 32 J.H. Forsmark, M. Li, X. Su, D.A. Wagner, J. Zindel, A.A. Luo, J.F. Quinn, R. Verma, Y.M. Wang, S.D. Logan, and S. Bilkhu, in *Magnesium Technology 2014*, ed. M. Alderman, M.V. Manuel, N. Hort, N.R. Neelamegham, (Switzerland: Springer International Publishing, 2016), p. 517.
- 33 G. Williams and H.N. McMurray, *Corrosion*, 62, 231 (2006).
- 34 S. Barbagallo, H.I. Laukli, O. Lohne, and E. Cerri, *J. Alloys Compd.*, 378, 226 (2004).
- 35 G. Williams, H. Ap Llwyd Dafydd, R. Subramanian, and H.N. McMurray, *Corrosion*, 73(5), 471 (2017).
- 36 Z.P. Cano, M. Danaie, J.R. Kish, J.R. McDermid, G.A. Botton, and G. Williams, *Corrosion*, 71, 146 (2015).
- 38 J.R. Kish, G. Williams, J.R. McDermid, J.M. Thuss, and C.F. Glover, *J. Electrochem. Soc.*, 161(9), C405 (2014).
- 39 M. Taheri, M. Danaie, and J.R. Kish, *J. Electrochem. Soc.*, 161(3), C89 (2014).

- 40 J.R. Kish, Y. Hu, J. Li, W. Zheng, and J.R. McDermid, *Corrosion*, 68(6), 468 (2012).
- 41 R. Tunold, H. Holtan, M.-B. Hägg Berge, A. Lasson, and R. Steen-Hansen, *Corros. Sci.*, 17, 353 (1977).
- 42 R.C Phillips and J.R. Kish, *Corrosion*, 69(8), 813 (2013).
- 43 J.W. Bocclair and P.S. Braterman, *Chem. Mater.*, 11, 298 (1999).
- 44 J.H. Nordlien, K. Nisancioglu, S. Ono, and N. Masuko, *J. Electrochem. Soc.*, 143(8), 2564 (1996).
- 45 J.H. Nordlien, K. Nisancioglu, S. Ono, and N. Masuko, *J. Electrochem. Soc.*, 144(2), 461 (1997).
- 46 S. Feliu, A. Pardo, M.C. Merino, A.E. Coy, F. Viejo, and R. Arrabal, *Appl. Surf. Sci.*, 255(7), 4102 (2009).